

Galaxy morphology in the rich cluster Abell 2390

J.B.Hutchings¹, A.Saintonge, D.Schade¹, D.Frenette

*Herzberg Institute of Astrophysics, National Research Council of Canada,
Victoria, B.C., Canada*

ABSTRACT

We have analysed images of the field of A2390 obtained with the CFHT and HST. The analysis fits models to bulge and disk components to several hundred galaxies, with about equal samples from the cluster and field. We also have assessed and graded asymmetries in the images. The cluster galaxies are compared in different cluster locations and also compared with field galaxies. We find that the central old population galaxies are bulge-dominated, while disk systems have young populations and are found predominantly in the outer cluster. S0 and bulgy disk galaxies are found throughout, but concentrate in regions of substructure. Disks of cluster blue galaxies are generally brighter and smaller than those in the field. We find that the cluster members have a higher proportion of interacting galaxies than the field sample. Interactions in the cluster and in the field, as well as cluster infall, appear to inhibit star-formation in galaxies.

Key words: galaxies: clusters: individual (A2390) — galaxies: fundamental parameters — galaxies: evolution

1. Introduction

The well-known rich cluster Abell 2390 at $z=0.23$ was studied as part of the CNOC1 cosmology program (Carlberg et al 1996). A detailed discussion of its spectroscopic properties from the CNOC1 database was published by Abraham et al (1996). From spectra of some 250 cluster galaxies, Abraham et al showed that infall into the cluster truncates star-formation, although there are some ‘near-field’ galaxies that have young populations, and may not yet be affected by the cluster environment.

The morphological structure of cluster galaxies is of interest in further understanding the effects of cluster infall and assimilation of galaxies. It is presumed that the high fraction

¹Guest Observer, Canada France Hawaii Telescope, which is operated by NRC of Canada, CNRS of France, and the University of Hawaii

of red central galaxies with old stellar populations are formed by tidal events that occur within the cluster, and giving them a bulge-dominated morphology. However, the CNOC1 imaging data were not used for a systematic morphological study until now.

In this paper, we have made use of a variety of additional imaging data of the cluster. We have performed a morphological modelling analysis of the cluster galaxies, and also of a field galaxy sample from the same databases. In our discussion we discuss the connection between morphology, cluster location, and spectra, and look for differences of properties in a similar sample of field galaxies.

The data used are from four databases. 1) the original CFHT MOS images from the CNOC1 database. These cover all the galaxies which have spectra, so are complete. However, the image quality and sampling are not optimal. 2) CFHT OSIS images have better sampling and image quality, from better observing conditions and with a tip-tilt imaging system. However, these images were part of a narrow-band imaging program and were not deeply exposed in the continuum band. 3) Images with the CFHT AO system in visible wavelengths produced still better sampled images with FWHM in the range 0.3 to 0.4". 4) Finally, we used HST WFPC2 images from our own and archival databases. These have FWHM about 0.2-0.3".

Table 1 summarizes the data and compares their coverage of the cluster. While the MOS data have the worst resolution, they offer the most extensive coverage of the cluster and have the highest signal level per pixel. Thus, in what follows, we have used the MOS data for most of the discussion, but have used the other datasets as checks on the morphology results. The analysis does create a PSF that may vary across the image fields, and uses them to calibrate the images, so that image resolution is not the overriding consideration for the images. While the OSIS data have superior resolution and sampling, their coverage of the cluster is less complete and the signal levels are much lower, so that they are not as useful. The PUEO and WFPC2 data are good quality checks on a limited subsample of galaxies.

2. Measurements

The galaxy images were classified using the software described by Schade et al (1996). Saintonge et al (2001) describe the analysis in detail for new data on some CNOC clusters, which is exactly the process followed for this discussion, including definitions of all quantities. Thus, we note only that the program was run on all data in Table 1. In the case of A2390, the model fits were all checked manually, rather than by an automatic checking process that was developed later for the larger datasets, based on the A2390 experience. In this process,

a uniform numerical criterion for model fit was applied in determining which models fits to include in the discussion.

While this eliminates poorly-defined models for faint or flawed images, it raises the question of whether a significant population of galaxies is rejected from our discussion. However, including lower quality model fits appears to increase noise in our plots rather than introducing clear systematic changes. More importantly, we applied the same criteria to the cluster and field galaxies, so the comparison between the two groups should not be affected.

In deciding to use the MOS data only for our discussion, we did a comparison of the results for the galaxies in common to the datasets. The correspondence was good between all pairs of measurements for galaxies whose data quality flags were good in both. The overall comparison of the principal measure (bulge/total light, or B/T) shows a mean difference of 0.02 over the range 0 to 1, with σ of 0.37, for all galaxies covered by more than one database. We have used the MOS data results restricted to only the good quality galaxy measurements. This amounts to 161 cluster galaxies, (of a total of 209 with spectroscopic measures) spread over a wide range of cluster positions (see Figure 1).

The process of fitting parametric models to these galaxies includes, as the first step, ‘symmetrizing’ the image to be fit. The galaxy image is rotated by 180° and subtracted from itself. The residuals are then clipped to leave only those portions of the residuals that are positive and that deviate by more than 2σ from symmetry. These high-significance residuals are then subtracted from the original image leaving a ‘symmetric’ image. This symmetric image is then fit by the models.

This process is very effective at removing the effects of companions and asymmetric features on the model-fitting process. It does not alter the possibility of separately classifying galaxy images as symmetric or asymmetric, and does not make classifications of interaction probability less effective. In fact, the asymmetric parts of the image were used in deriving the interaction index, described below.

A central question is whether many of the interacting galaxies have been removed from the sample because we are presenting only ‘good’ fits. While there may be a few such galaxies that have been rejected, the symmetrizing process makes it less likely that we have rejected very many moderately (or less) interacting galaxies. We stress again that the comparison between field and cluster is done with the same criteria for inclusion.

We combined two field-galaxy samples for comparison: galaxies from the A2390 images with redshifts (mostly in the range 0.16 to .35, so comparable with the cluster redshift of 0.23); and field galaxies in the redshift range 0.19 to 0.27 using MOS images from other

CNOC clusters. These datasets contained 97 and 111 galaxies, respectively. Almost all the cluster and field galaxies in our morphological database have spectra from the CNOC1 program, and we have thus combined the morphological and spectroscopic measurements from Abraham et al (1996) in some of the discussions that follow.

We examined the best (MOS and OSIS) galaxy images (and their asymmetries as isolated by rotation) and classified their ‘interaction level’, based on the distinctness of tidal tails, connecting luminosity, warped disks, off-centre nuclei, and other asymmetries, with reference to a grid of models of galaxy interactions computed with a tree code. This classification was done independently by two of us for a subset of galaxies to standardize the criteria, and the results are given for the full set on a 5-point scale. A similar classification was described in more detail by Hutchings and Neff (1991).

Finally, we made a measure of the local galaxy density by counting the distance to the 10th-nearest neighbour galaxies on the sky. The density value used was proportional to the log of the inverse square of this radius. This enabled us to investigate the effects of local galaxy density independently of clustocentric radius (although without correction for non-member galaxies).

Tables 2 and 3 show the values used in this paper for cluster and field galaxies. In the sections below we present and discuss the more significant correlations among the morphology, spectroscopic, photometric, and positional measures of the cluster and field galaxies. Where sizes and luminosities are shown, we have used $H_0=50$ and $q_0=0.5$.

3. Cluster galaxy morphologies

Abraham et al (1996) discussed the spectroscopic and photometric properties of the cluster in considerable detail. The diagrams in the present paper illustrate the morphological parameters of the cluster galaxies, as they relate to the spectroscopic and photometric data, and to their position in the cluster. The principal properties we discuss are the bulge to disk flux ratio, and some aspects of their sizes and luminosities.

Figure 1 shows the spatial distribution of the cluster galaxies in the sample. We have in general divided the galaxies into 3 types: ‘bulge’, which has modelled bulge/total light (B/T) of 0.8 or larger; ‘disk’ which has B/T less than 0.4, and ‘S0’, which has B/T between 0.4 and 0.8. The intermediate classification probably contains all S0 type galaxies, but will also include others such as Sa with a bright bulge. The sample extends to large distances from the centre, along the principal axis of extension of the cluster. The top panel shows the MOS results which we have used, as discussed above. The lower panel shows the distribution

of the galaxies in the other datasets analysed. The OSIS data have gaps at intermediate radii, and are much noisier, while the PUEO and HST data cover only the central region.

Figure 2 shows the spatial distribution of B/T with normalised radius within the cluster. (The normalised radius is defined as the radius within the cluster as a fraction of R200, the radius at which the cluster density is 200 times the critical density.) It also shows the same for the field sample, plotted with redshift mainly as a way to spread the points out (but does also show that we have no strong redshift-dependent effects). The field galaxies bracket the cluster redshift of 0.23 in any case.

The gap in the B/T distribution is caused by an explicit bias. In those cases where a single component model (e.g. pure disk or pure bulge) is indistinguishable statistically from a two-component model (bulge plus disk) then we adopt the single component model. In the region $B/T > 0.8$ (roughly) the bulge clearly dominates the luminosity profile and it is frequently difficult to detect a disk even if one is present (as determined from simulations). Furthermore, the measured parameters of the bulge are affected very little by the choice of pure bulge or bulge-plus-disk model. In these cases too, we choose the single-component model.

The size of the gap in the B/T diagram depends on signal-to-noise ratio. If the observations all had very high S/N then there would be no gap because it would be possible to detect even very weak disks in the presence of dominant bulges.

In Figure 2, there are clearly separate populations of bulge galaxies that are not a continuation of the trends seen in the pure disk through increasing bulge up to B/T 0.8. This bulge population is more marked in the cluster, as expected, but galaxies are found at all projected radii within the cluster. There are more disk-dominated galaxies in the field, also as expected.

In Figure 3 we show the distributions of intrinsic colour with disk surface brightness for the two samples, which differ significantly. The dotted lines mark the mean values from the field sample, which are fairly evenly spread about these values. The greater spread to bluer colours reflect the redshift range, which limits the observed red colour of the galaxies. The cluster galaxy distribution is mainly skewed by the cluster red sequence, but also shows a paucity of low surface brightness disks among the blue galaxies.

In Figure 4 we compare the disk scale-lengths. These are related to the absolute magnitude, with brighter galaxies having bigger disks. The dotted line is the linear fit to the log-log plot for field galaxies. The cluster galaxies distribution differs from this as illustrated by the dashed curve, which is a second order fit to the points: the disks are generally smaller (as well as brighter as seen in Figure 3), but there is a tail of larger disks that are the brightest

ones in Figure 3.

Figure 5 shows the distribution of galaxy types plotted with local galaxy density. This is strongly correlated with radius within the cluster, as shown by the radius values in the plot: the density is highest in the cluster centre and falls with radius in the inner cluster. Beyond that there is a region where radius and density appear largely unrelated. The outer cluster shows a clear monotonic decline in density. Figure 5 has bins that separate these three regions, with the central region divided into two bins of equal numbers of member galaxies. The plot shows what is generally expected: the central regions strongly dominated by bulge galaxies, and a rising disk fraction with radius. The ‘S0’ population remains near to 20% at all radii.

Figure 6 compares some key spectroscopic measures with the B/T ratio. These are the stellar population indicators used by Abraham et al (1996). We have included all galaxies with good morphology measures but they are not filtered by spectroscopic data quality, since these are not readily available for the assembled field sample. The D4000 data are, however, separated for the brightest galaxies, which will have better spectroscopic data as well. There are some differences, as follows.

The [O II] emission, a signature of hot star formation, is somewhat suppressed compared with the field galaxies, but has a wider range. The differences are larger for lower B/T values. H δ absorption, a post-starburst measure, is stronger for the cluster galaxies, again more noticeably for the lower B/T values. D4000, a measure of old stellar populations, is larger for the cluster galaxies, and more so for the intermediate B/T values. All these are consistent with the idea proposed by Abraham et al (1996) for this cluster, and Morris et al (1998) for another CNOC cluster, namely that infall into the cluster truncates star-formation.

Figure 7 plots the spectroscopic indices with our estimates of interaction strength for cluster and field galaxies. This plot shows the overall differences discussed for Figure 6, and also illustrates connections to disturbed galaxy morphology. The distributions in Figure 7 show significant difference between cluster and field galaxies in all comparisons. The numbers on the right show the differences in percent of each sample in each interactions subset: the cluster galaxies appear to be more interacting than the field sample, again as expected.

In the spectroscopic measures in Figure 7, [O II] emission is stronger in the field sample, but both samples show decreased emission for stronger interactions. This suggests that interactions inhibit star-formation in all environments that are covered. H δ absorption is also stronger in field galaxies, increasing with tidal interaction. The cluster galaxies show a small trend the other way — less H δ in highly interacting systems. The D4000 index decreases with interaction in both samples, but there is a strong difference between field and

cluster galaxies.

4. Discussion

We find that the morphology measurements of A2390 cluster galaxies generally support the expectations of the spectroscopic analysis by Abraham et al (1996). The red central galaxies are bulge-dominated systems, as expected from their old stellar populations. Such galaxies are strongly concentrated in the cluster core. Disk systems on the other hand are increasingly dominant in outer parts of the cluster. The S0 (and other bulgy disks) are found at all radii, but seem to be associated with regions of subclumps within the cluster. This is consistent with their being stripped disk galaxies as a result of recent infall into the cluster. 50% of the field galaxies are disk-dominated (B/T=0), while the cluster galaxies are dominated by the bulge-only (B/T=1) population. The distribution of intermediate B/T values is similar for the two samples, but they may refer to different morphologies (S0 and Sa, say) which we cannot distinguish.

The cluster disks are mostly fainter and smaller than the field galaxy disks, which is presumably also a result of tidal or stripping effects of infall. The few bright large disks are found in galaxies spread across the cluster, with no particular other properties.

The spectroscopic properties (Figures 6 and 7) indicate that the disk-dominated systems have post-starburst stellar populations, compared with the field sample, while the bulge-dominated galaxies are very similar in cluster and field. This too supports the conclusion that infall into the cluster truncates star-formation. The interaction statistics add some more information to this: interactions are more common among the cluster galaxies, as expected, but in both field and cluster samples, the [O II] is increasingly suppressed with increased interaction visibility. Thus, this truncation of star-formation appears to happen in non-cluster environments too (although significantly more marked in the cluster).

If we regard the interaction visibility as an indicator of the age of a tidal event, the H δ data suggest a sequence of post-starburst populations, again with the effects more marked in the cluster sample.

Abraham et al (1996) noted a few near-field galaxies that appear to be in the early stages of infall. These are blue and have young stellar populations. Our morphology measures for these galaxies show them to be disk-dominated, but with other properties that are varied but typical of the distribution of cluster galaxies. We have thus simply included them as cluster galaxies in our diagrams.

We are grateful to M. Balogh for making the OSIS images available to us while still proprietary.

Table 1. Comparison of the different data sets

Data	Field of view (# fields)	FWHM (")	Pixel size (")	Exp time (sec)	Band	#galx ¹	sig/pixel ²
MOS	10' × 10' (5)	0.99	0.315	900	R	236	1160
OSIS	4.1' × 3.4' (19)	0.64	0.155	90	R	173	30
PUEO	2' × 2' (1)	0.43	0.061	1200x3	I	13	170
WFPC2	2.5' × 2.5' (3)	0.18	0.105	2100x5	(I)	26	350

¹Number of galaxies with morphology measurements

²Proportional to the product of telescope throughput, exposure, and pixel area on sky.

Table 2. Cluster galaxies

z	M_B	r_{norm} (Mpc)	(U-V) ₀	B/T	μ_{disk}	μ_{bulge}	Scl.ht log(kpc)	1/2lt rad log(kpc)	[OII] (Å)	H_δ (Å)	D4000	Int level
0.2316	-18.70	0.04	1.88	1.	...	12.2	...	0.30	3.4	-0.9	2.16	0.
0.2238	-19.45	0.04	1.98	0.56	19.8	14.6	0.29	0.69	4.8	3.4	2.50	3.
0.2150	-19.66	0.04	2.04	0.59	19.7	12.0	0.30	0.22	-1.5	0.8	2.62	2.
0.2284	-19.42	0.04	1.99	1.	...	11.6	...	0.25	0.6	-1.0	2.87	...
0.2178	-18.00	0.04	2.21	0.	20.9	...	0.36	...	-14.9	2.8	1.87	...
0.2304	-18.33	0.04	1.99	1.	...	12.2	...	0.13	3.2	2.9	2.49	1.
0.2237	-17.92	0.05	2.01	1.	...	12.9	...	0.35	-5.1	-6.4	1.64	...
0.2551	-20.20	0.05	1.80	0.69	24.0	13.3	1.27	0.69	2.5	0.7	2.51	...
0.2203	-20.15	0.06	1.89	0.56	22.4	12.5	0.94	0.41	6.9	1.0	2.51	0.
0.2470	-19.08	0.07	1.91	0.27	19.9	12.8	0.35	0.09	1.2	-2.9	2.20	1.
0.2188	-19.48	0.08	1.95	0.36	20.8	11.2	0.58	-0.07	-6.0	-2.8	2.81	0.
0.2303	-18.56	0.08	1.77	1.	...	11.9	...	0.25	1.4	-2.0	2.19	1.
0.2192	-19.85	0.08	1.92	1.	...	12.8	...	0.61	3.6	-1.2	2.94	3.
0.2244	-18.05	0.09	1.83	0.52	22.0	9.7	0.47	-0.58	5.2	1.4	2.38	0.
0.2292	-18.63	0.10	1.77	1.	...	12.1	...	0.49	-3.0	3.1	2.08	0.
0.2214	-19.26	0.11	1.93	1.	...	12.7	...	0.46	14.4	0.2	2.65	...
0.2461	-18.68	0.11	1.84	1.	...	13.5	...	0.50	0.1	4.1	2.52	4.
0.2287	-19.27	0.12	1.84	1.	...	13.3	...	0.67	0.9	2.8	2.50	...
0.2363	-19.29	0.12	1.82	0.22	21.0	8.1	0.64	-0.82	-0.2	0.8	2.67	...
0.2221	-19.11	0.13	1.83	1.	...	12.0	...	0.61	6.5	0.9	2.53	...
0.2288	-19.61	0.14	2.04	1.	...	13.2	...	0.79	-0.1	2.5	2.07	2.
0.2199	-18.79	0.14	1.24	1.	...	11.1	...	0.29	-1.0	6.3	1.92	1.
0.2422	-18.48	0.14	1.89	0.39	20.8	12.4	0.37	-0.02	-3.9	1.4	2.29	4.
0.2281	-19.83	0.14	1.92	1.	...	11.9	...	0.67	4.9	-1.9	2.67	0.
0.2294	-19.24	0.16	1.90	1.	...	12.7	...	0.75	6.9	-1.2	2.28	2.
0.2313	-19.97	0.18	1.90	0.24	20.6	7.3	0.68	-0.84	-4.6	-1.2	3.30	0.
0.2302	-18.10	0.18	1.94	0.51	23.4	14.0	0.83	0.34	-26.8	7.5	2.31	0.
0.2238	-19.32	0.19	2.01	0.63	21.2	11.7	0.51	0.12	3.6	-1.2	2.87	0.
0.2221	-18.26	0.20	1.56	1.	...	12.5	...	0.39	-6.3	5.6	2.39	...
0.2253	-20.15	0.20	1.59	0.2	20.5	7.2	0.72	-0.85	1.1	5.6	2.01	3.
0.2319	-19.01	0.21	1.92	0.57	20.5	13.9	0.34	0.49	-6.2	1.2	2.48	...
0.2322	-20.23	0.22	1.93	0.44	21.8	12.2	0.94	0.33	4.6	-0.8	2.63	...
0.2328	-18.23	0.22	1.80	0.28	20.4	8.8	0.31	-0.84	-14.7	1.5	1.88	0.
0.2324	-18.88	0.22	1.86	0.34	20.7	11.5	0.45	-0.14	4.8	-4.6	2.43	...
0.2354	-18.97	0.24	1.85	0.1	21.6	12.1	0.71	-0.28	4.9	0.4	1.88	0.
0.2305	-19.52	0.24	1.86	1.	...	13.5	...	0.65	0.5	-2.5	2.61	...
0.2251	-19.67	0.24	1.95	1.	...	12.6	...	0.50	-9.0	-1.3	3.26	...
0.2294	-18.85	0.24	1.91	0.75	21.4	15.5	0.41	0.85	-25.7	-5.4	2.86	3.
0.2290	-18.60	0.24	1.16	0.44	20.8	13.3	0.41	0.25	-9.6	8.3	2.13	1.
0.2295	-18.91	0.25	1.90	0.46	21.2	9.8	0.52	-0.41	11.3	4.0	2.33	...
0.2224	-17.79	0.26	1.85	1.	...	14.1	...	0.45	3.5	3.1	1.85	3.
0.2237	-19.61	0.27	1.92	0.29	20.5	8.8	0.57	-0.58	16.9	1.1	2.18	...
0.2245	-19.77	0.27	1.78	0.25	20.8	8.3	0.69	-0.66	4.6	-0.6	2.67	...
0.2318	-18.62	0.28	1.95	0.24	20.9	8.7	0.46	-0.84	9.0	3.2	2.58	3.
0.2246	-17.92	0.29	2.06	1.	...	13.0	...	0.28	8.4	4.2	3.09	2.
0.2318	-18.89	0.29	1.85	0.7	23.4	13.2	0.83	0.37	13.1	6.8	2.14	2.
0.2202	-18.95	0.30	1.92	1.	...	11.7	...	0.45	10.3	2.1	2.04	3.

Table 2—Continued

z	M_B	r_{norm} (Mpc)	(U-V) ₀	B/T	μ_{disk}	μ_{bulge}	Scl.ht log(kpc)	1/2lt rad log(kpc)	[OII] (Å)	H_δ (Å)	D4000	Int level
0.2283	-19.32	0.30	1.50	0.	20.6	...	0.64	...	11.0	1.4	2.49	2.
0.2251	-18.15	0.30	1.33	0.	20.4	...	0.35	...	-4.4	-6.9	1.43	1.
0.2253	-20.76	0.30	1.85	1.	...	14.3	...	1.11	-6.9	-1.7	2.72	...
0.2237	-18.99	0.31	1.95	0.16	21.1	8.9	0.58	-0.83	-5.8	-0.5	2.44	0.
0.2350	-19.24	0.32	1.90	1.	...	14.3	...	0.83	20.1	7.6	2.44	...
0.2285	-19.19	0.32	1.71	0.4	19.9	7.6	0.31	-0.84	0.1	2.6	2.35	...
0.2300	-19.11	0.32	1.94	0.36	20.4	8.2	0.44	-0.74	14.1	-0.5	2.36	1.
0.2211	-18.09	0.32	1.67	0.	22.8	...	0.83	...	-46.1	12.2	1.44	1.
0.2235	-20.02	0.32	1.78	0.27	20.8	7.2	0.72	-0.83	-5.4	0.9	2.45	0.
0.2226	-19.59	0.33	1.86	1.	...	11.9	...	0.57	-12.0	2.3	2.50	...
0.2265	-18.28	0.33	1.86	1.	...	12.0	...	0.15	1.2	3.2	2.21	...
0.2275	-18.55	0.33	1.75	1.	...	12.8	...	0.68	4.2	-3.5	3.43	1.
0.2292	-18.43	0.33	1.93	0.29	21.3	8.7	0.47	-0.84	16.5	4.7	2.46	0.
0.2314	-17.12	0.34	1.14	0.42	24.1	12.7	0.92	-0.03	58.7	-0.7	3.70	0.
0.2293	-18.94	0.34	1.63	0.	20.3	...	0.52	...	-6.2	-0.7	1.89	...
0.2248	-18.59	0.35	1.52	0.12	20.3	9.4	0.40	-0.84	2.3	3.9	1.99	...
0.2220	-19.58	0.35	1.92	0.3	21.5	10.1	0.73	-0.33	-2.9	3.7	2.12	...
0.2341	-19.26	0.35	1.84	1.	...	11.0	...	0.24	4.6	1.7	2.25	...
0.2433	-17.70	0.35	1.76	1.	...	11.8	...	0.09	-4.5	6.8	2.13	1.
0.2313	-17.87	0.36	1.87	1.	...	13.2	...	0.43	50.5	6.9	3.92	0.
0.2287	-18.59	0.36	1.68	1.	...	13.4	...	0.55	-13.5	-0.4	2.59	...
0.2253	-19.19	0.36	1.87	0.53	21.8	10.7	0.64	-0.15	20.5	-2.6	3.34	2.
0.2166	-19.32	0.36	1.99	0.21	20.4	8.4	0.47	-0.84	4.5	-0.2	2.53	...
0.2388	-18.63	0.36	1.45	0.	19.5	...	0.27	...	3.9	4.3	2.07	0.
0.2322	-19.56	0.36	2.02	0.51	22.4	11.8	0.87	0.14	4.1	-0.7	2.65	...
0.2269	-19.71	0.37	1.93	0.52	22.9	12.5	0.99	0.32	12.0	0.8	3.05	1.
0.2158	-19.38	0.38	1.74	0.18	21.1	11.8	0.67	-0.12	3.5	2.2	2.32	3.
0.2253	-17.40	0.38	1.15	0.	20.2	...	0.16	...	-17.7	4.8	1.59	3.
0.2266	-18.62	0.39	1.78	1.	...	13.5	...	0.50	12.6	2.1	2.09	...
0.2311	-18.76	0.40	1.90	0.51	21.7	13.2	0.57	0.27	-2.8	-2.6	2.40	0.
0.2409	-18.41	0.40	1.89	0.38	21.6	11.7	0.53	-0.17	-27.1	-3.8	2.18	0.
0.2245	-18.46	0.40	2.04	0.39	21.6	12.9	0.51	0.07	-3.1	2.6	3.22	3.
0.2321	-18.44	0.41	1.90	0.35	20.5	11.3	0.33	-0.25	16.6	0.6	2.34	...
0.2247	-18.72	0.43	1.26	0.	19.8	...	0.37	...	9.3	7.1	1.84	...
0.2427	-18.16	0.44	0.85	0.07	21.3	10.1	0.59	-0.84	0.7	3.8	1.62	2.
0.2282	-18.39	0.47	1.77	1.	...	13.0	...	0.64	7.4	-0.8	2.69	4.
0.2223	-18.93	0.51	1.93	0.3	21.1	11.5	0.57	-0.16	37.5	-2.0	3.32	...
0.2366	-17.30	0.51	1.52	0.	21.2	...	0.36	...	7.8	2.0	2.14	0.
0.2280	-18.19	0.53	1.81	0.	19.7	...	0.21	...	6.9	4.8	3.08	2.
0.2237	-18.91	0.58	1.76	1.	...	12.6	...	0.39	0.9	1.0	2.40	0.
0.2313	-18.89	0.60	1.82	0.33	21.8	12.8	0.71	0.15	-13.2	3.7	1.77	...
0.2302	-18.90	0.60	1.14	0.	20.2	...	0.49	...	-17.7	2.5	1.46	1.
0.2217	-19.86	0.62	1.44	0.22	18.5	8.3	0.28	-0.65	-3.7	3.1	1.67	1.
0.2235	-19.76	0.62	1.95	1.	...	12.7	...	0.60	1.7	-7.6	2.39	0.
0.2155	-18.75	0.63	1.20	0.	21.4	...	0.72	...	-44.4	4.3	1.61	1.
0.2324	-18.94	0.63	1.68	0.36	20.8	14.6	0.51	0.53	6.9	3.4	1.96	0.
0.2334	-18.51	0.64	1.83	0.	20.0	...	0.36	...	-12.6	6.1	2.19	...

Table 2—Continued

z	M_B	r_{norm} (Mpc)	(U-V) ₀	B/T	μ_{disk}	μ_{bulge}	Scl.ht log(kpc)	1/2lt rad log(kpc)	[OII] (Å)	H_δ (Å)	D4000	Int level
0.2253	-19.63	0.64	1.45	0.	20.0	...	0.60	...	-5.8	6.9	1.81	...
0.2351	-19.85	0.66	1.80	0.42	21.3	11.7	0.74	0.13	7.8	1.1	2.53	...
0.2323	-19.02	0.68	1.84	1.	...	11.9	...	0.47	0.9	2.7	2.36	3.
0.2278	-18.53	0.69	1.17	0.	20.2	...	0.42	...	-12.7	5.3	1.76	...
0.2257	-18.74	0.71	1.90	1.	...	12.4	...	0.55	2.6	2.0	2.00	...
0.2326	-17.82	0.71	1.56	0.	20.7	...	0.37	...	-9.9	6.9	2.10	...
0.2240	-20.09	0.72	1.83	0.57	21.0	14.2	0.68	0.77	3.0	-1.0	2.69	1.
0.2230	-18.46	0.72	1.91	1.	...	11.2	...	-0.02	-22.3	-0.2	2.71	...
0.2279	-19.25	0.73	1.60	1.	...	13.5	...	0.65	-2.5	3.2	1.96	0.
0.2312	-19.16	0.73	1.90	0.43	22.3	12.1	0.83	0.13	21.4	1.2	2.27	...
0.2239	-18.73	0.76	1.96	0.31	20.8	10.0	0.44	-0.50	75.2	-4.9	2.70	...
0.2265	-17.60	0.77	1.75	0.	20.0	...	0.14	...	5.7	3.6	2.32	...
0.2248	-19.15	0.77	1.10	0.	19.9	...	0.50	...	5.2	2.8	1.63	0.
0.2279	-17.21	0.77	0.74	0.	21.0	...	0.37	...	-21.2	12.	1.64	...
0.2254	-18.66	0.78	1.78	1.	...	13.7	...	0.63	-12.8	2.9	1.74	...
0.2183	-18.21	0.80	1.66	1.	...	13.3	...	0.60	-9.6	1.8	2.47	...
0.2341	-19.33	0.81	1.84	1.	...	12.7	...	0.58	4.9	-2.6	2.39	...
0.2331	-17.84	0.82	1.86	1.	...	13.2	...	0.27	45.2	4.6	1.96	...
0.2257	-17.41	0.82	1.18	0.	21.4	...	0.49	...	-26.1	12.1	1.57	...
0.2228	-19.19	0.84	1.64	1.	...	12.9	...	0.50	-9.1	-2.7	1.76	0.
0.2163	-19.55	0.86	1.76	0.53	20.6	12.0	0.51	0.20	9.0	3.9	2.41	0.
0.2332	-18.72	0.87	1.77	1.	...	14.8	...	0.87	6.0	4.4	2.55	2.
0.2469	-19.25	0.90	1.79	1.	...	14.1	...	0.79	6.3	1.0	2.77	2.
0.2271	-18.82	0.90	1.58	0.61	20.2	15.1	0.30	0.76	-13.6	0.5	1.95	...
0.2371	-18.49	0.90	1.63	0.05	21.5	10.3	0.65	-0.84	-3.7	5.6	2.15	2.
0.2302	-17.75	0.90	1.71	0.	20.0	...	0.17	...	3.8	4.9	2.38	3.
0.2284	-17.26	0.91	1.59	0.	20.9	...	0.28	...	4.9	0.3	2.21	1.
0.2199	-18.73	0.94	1.78	0.	20.7	...	0.52	...	1.6	3.6	2.43	...
0.2286	-19.49	0.94	1.82	0.23	21.5	15.9	0.78	0.79	8.0	2.6	2.34	...
0.2329	-19.63	0.95	1.40	0.12	20.1	8.2	0.57	-0.84	-8.5	2.5	1.65	...
0.2282	-19.58	0.95	2.08	0.25	22.5	12.8	1.06	0.27	-5.9	15.7	2.38	3.
0.2348	-19.41	0.96	1.84	1.	...	14.5	...	0.88	-6.0	4.8	2.44	1.
0.2249	-19.79	0.97	1.85	0.59	22.0	10.9	0.80	0.05	2.8	-2.2	2.58	...
0.2284	-18.83	0.97	1.84	1.	...	13.8	...	0.78	6.2	4.2	2.23	0.
0.2363	-18.24	0.97	1.70	0.	19.9	...	0.27	...	4.7	3.9	2.10	...
0.2265	-19.67	0.99	1.89	0.65	23.1	13.0	0.96	0.45	-3.3	3.5	2.75	...
0.2269	-18.80	0.99	1.71	0.39	20.5	9.5	0.39	-0.53	6.8	4.0	2.27	...
0.2233	-19.23	1.00	1.87	0.08	21.0	9.2	0.67	-0.84	-16.9	-1.9	2.46	1.
0.2251	-19.47	1.05	1.75	0.06	21.4	9.3	0.81	-0.82	-1.2	6.0	2.22	0.
0.2274	-17.65	1.06	1.73	1.	...	15.1	...	0.74	-16.4	-0.3	2.10	1.
0.2353	-20.24	1.07	1.86	0.39	21.4	11.1	0.83	0.06	1.3	-1.7	2.45	2.
0.2244	-18.43	1.13	1.53	0.61	21.0	13.9	0.35	0.40	7.3	9.6	2.12	3.
0.2287	-19.40	1.13	1.58	0.18	20.2	8.2	0.51	-0.47	-9.2	4.4	2.13	0.
0.2315	-19.30	1.14	1.60	0.18	20.1	14.5	0.50	0.45	3.0	3.9	1.88	1.
0.2226	-19.41	1.15	1.88	0.13	20.9	9.5	0.74	-0.56	-1.2	1.2	2.20	1.
0.2354	-19.12	1.15	1.78	1.	...	12.2	...	0.62	3.1	0.0	2.61	...
0.2301	-19.33	1.16	1.86	0.39	21.1	7.4	0.60	-0.84	4.7	-1.2	2.81	...

Table 2—Continued

z	M_B	r_{norm} (Mpc)	(U-V) ₀	B/T	μ_{disk}	μ_{bulge}	Scl.ht log(kpc)	1/2lt rad log(kpc)	[OII] (Å)	H_δ (Å)	D4000	Int level
0.2345	-18.33	1.17	1.78	0.63	20.9	13.5	0.28	0.31	2.1	1.0	2.06	4.
0.2544	-19.66	1.18	1.88	0.53	23.0	11.4	0.99	0.10	-5.5	3.7	2.31	0.
0.2290	-19.23	1.20	1.37	1.	...	14.1	...	0.85	0.8	0.5	...	2.
0.2248	-18.03	1.20	1.59	1.	...	14.0	...	0.80	-50.3	8.1	2.60	...
0.2599	-18.22	1.27	1.61	1.	...	12.8	...	0.26	9.8	5.4	2.27	1.
0.2254	-18.50	1.29	1.53	0.	20.2	...	0.38	...	-8.6	4.1	2.08	0.
0.2265	-18.72	1.31	1.78	1.	...	11.7	...	0.28	6.9	1.6	2.16	0.
0.2291	-19.38	1.35	1.53	0.	20.8	...	0.67	...	-7.2	3.7	2.13	...
0.2267	-18.86	1.35	1.84	1.	...	12.9	...	0.60	7.9	-0.4	2.33	1.
0.2357	-18.40	1.35	1.62	0.	20.5	...	0.43	...	-45.5	5.8	1.83	1.
0.2232	-19.91	1.42	1.84	1.	...	14.1	...	0.96	6.6	1.3	2.39	...
0.2287	-19.05	1.47	1.75	1.	...	12.6	...	0.52	4.5	0.2	2.63	0.
0.2228	-19.65	1.50	1.83	0.42	21.3	10.6	0.70	-0.12	-2.0	1.7	2.70	4.
0.2333	-18.85	1.58	1.77	1.	...	12.9	...	0.64	0.3	3.1	2.64	...
0.2221	-18.99	1.63	1.60	1.	...	13.4	...	0.63	-1.2	6.8	1.71	...
0.2227	-17.74	1.70	1.56	1.	...	13.5	...	0.35	4.0	1.8	1.98	1.
0.2232	-18.91	1.79	0.75	0.	19.6	...	0.40	...	-16.1	2.4	1.46	...
0.2133	-18.09	1.87	1.69	1.	...	13.5	...	0.41	5.5	4.0	2.03	4.
0.2329	-18.78	1.88	1.16	0.13	20.6	12.9	0.53	-0.04	8.0	8.4	2.07	2.
0.2252	-18.80	2.10	2.01	0.09	20.7	11.1	0.50	-0.54	-22.7	4.1	2.22	1.

Table 3. Field Galaxies

z	M_B	$(U-V)_0$	B/T	μ_{disk}	μ_{bulge}	Scl.ht log(kpc)	1/2lt rad log(kpc)	$[OII]$ (\AA)	H_δ (\AA)	D4000	Int level
0.0658	-17.77	0.84	0.	18.52	...	-0.1	0.
0.0669	-14.34	0.59	0.47	20.51	10.21	-0.6	-1.3	...	6.5	...	0.
0.0683	-14.83	1.50	0.	20.76	...	-0.3	9.8
0.1029	-17.80	1.24	0.	20.83	...	0.3	16.4
0.1149	-20.06	2.14	1.	...	13.45	...	0.7	...	2.0
0.1264	-18.00	2.45	0.47	21.77	10.46	0.3	-0.6	...	-17.7	...	0.
0.1472	-17.76	1.30	0.	20.65	...	0.3	6.6	1.47	...
0.1588	-19.46	1.37	0.37	20.66	14.06	0.5	0.5	...	5.7	1.74	4.
0.1689	-18.03	1.79	1.	...	10.91	...	0.2	...	1.3	2.11	...
0.1699	-20.72	1.57	1.	...	16.12	...	1.6	...	6.9	1.83	...
0.1740	-18.71	1.39	0.	20.24	...	0.4	6.2	1.70	...
0.1755	-18.51	1.97	0.31	20.27	11.13	0.3	-0.3	...	0.5	2.19	...
0.1783	-16.90	1.70	0.	19.46	...	-0.1	...	12.3	7.8	1.49	1.
0.1785	-20.57	2.00	0.43	21.92	12.71	1.0	0.5	1.8	-0.4	2.41	...
0.1794	-20.05	1.58	0.2	19.84	15.06	0.5	0.7	-36.	2.8	2.64	...
0.1796	-19.42	2.05	0.31	20.85	9.99	0.6	-0.4	-3.	1.2	2.42	...
0.1799	-19.25	2.17	0.07	21.6	11.19	0.7	-0.5	17.2	11.2	1.57	...
0.1800	-17.63	1.70	0.	19.65	...	0.1	...	-20.3	2.3	1.88	...
0.1851	-18.45	1.91	0.31	21.34	8.81	0.5	-0.8	-29.7	0.0	2.52	...
0.1861	-18.05	1.80	0.	19.84	...	0.2	...	-8.5	7.2	1.78	...
0.1879	-17.95	0.98	0.	20.36	...	0.3	...	-38.3	4.4	1.77	1.
0.1898	-19.08	2.19	0.77	21.12	14.94	0.3	0.7	-0.42	2.
0.2028	-18.18	1.56	0.	19.93	...	0.2	...	-22.5	4.5	1.83	...
0.2032	-18.12	1.26	1.	...	12.65	...	0.3	-13.6	5.5	1.88	...
0.2047	-19.50	1.12	0.	20.04	...	0.6	...	-9.3	12.6	1.90	...
0.2060	-18.81	1.52	0.03	21.75	10.27	0.8	-0.9	-24.5	6.5	1.97	...
0.2544	-18.52	1.61	1.	...	11.68	...	0.2	3.3	0.5	2.30	0.
0.2551	-20.30	1.55	0.76	19.84	14.77	0.4	1.	-3.7	6.9	2.01	...
0.2579	-17.95	0.71	0.	21.3	...	0.5	...	-51.3	4.0	1.48	...
0.2599	-18.54	0.69	0.	20.54	...	0.5	...	-7.5	5.9	1.66	1.
0.2617	-17.54	2.15	0.14	22.62	16.17	0.7	0.4	-13.4	-10.8	1.34	...
0.2646	-17.45	0.73	0.	20.01	...	0.2	...	-46.2	5.1	1.43	...
0.2654	-18.28	0.97	0.	21.24	...	0.6	...	-14.1	1.9	1.91	...
0.2661	-16.92	0.95	0.	19.04	...	-0.1	...	-74.7	6.6	1.86	0.
0.2741	-18.86	1.32	0.	19.65	...	0.4	...	-1.6	6.5	1.83	0.
0.2745	-18.51	1.52	1.	...	20.21	...	2.	-4.1	0.7	1.96	...
0.2751	-16.63	0.63	0.	24.76	...	1.5	...	-63.3	9.4	1.14	...
0.2797	-19.75	1.42	0.1	21.08	8.45	0.8	-0.8	-7.5	4.1	2.11	0.
0.2810	-20.16	1.64	0.25	21.48	11.76	0.9	0.2	-6.8	-0.4	1.97	1.
0.2819	-19.78	1.48	1.	...	14.94	...	1.2	-5.6	3.5	1.81	1.
0.2827	-16.85	1.00	0.	20.	...	0.1	...	-43.7	7.9	2.03	...
0.2834	-18.43	1.10	0.	20.93	...	0.6	...	-9.	8.1	1.69	0.
0.3042	-17.53	1.36	0.89	22.8	9.67	0.3	-0.5	-9.	-1.0	1.91	...
0.3066	-20.06	1.75	0.09	21.02	8.32	0.9	-0.7	-7.5	-1.4	1.92	...
0.3068	-17.53	0.65	0.	20.33	...	0.7	...	-28.3	11.1	1.97	...
0.3069	-17.94	1.28	0.77	27.52	11.64	1.5	0.	-22.5	4.1	1.76	...
0.3071	-19.58	1.05	0.	20.47	...	0.7	...	-11.6	2.0	2.09	2.

Table 3—Continued

z	M_B	$(U-V)_0$	B/T	μ_{disk}	μ_{bulge}	Scl.ht log(kpc)	1/2lt rad log(kpc)	$[OII]$ (\AA)	H_δ (\AA)	D4000	Int level
0.3076	-17.83	0.92	0.	20.99	...	0.5	...	-34.1	4.7	2.09	3.
0.3077	-19.71	1.17	0.22	22.24	14.15	1.1	0.6	-8.0	1.0	1.77	...
0.3080	-18.66	1.17	0.	19.99	...	0.5	...	-26.8	3.3	1.75	1.
0.3093	-17.75	0.60	0.	19.31	...	0.1	...	-40.1	5.3	1.39	...
0.3093	-17.26	0.54	0.	21.08	...	0.4	...	-38.4	10.3	1.41	1.
0.3097	-17.74	1.79	0.22	25.81	9.81	1.6	-0.5	5.2	0.4	1.93	...
0.3125	-17.82	0.67	1.	...	14.53	...	0.9	-33.6	9.5	1.35	...
0.3149	-18.23	1.04	0.	20.4	...	0.4	...	-21.4	12.	1.79	...
0.3167	-20.28	1.87	0.37	21.32	11.6	0.9	0.2	-12.9	-3.6	2.86	...
0.3179	-20.04	1.63	1.	...	14.44	...	1.2	-11.6	-0.7	2.15	...
0.3199	-20.11	1.86	0.63	22.78	12.39	1.1	0.5	-4.1	-0.4
0.3203	-18.87	1.19	0.	20.3	...	0.6	...	-15.	9.3	...	3.
0.3207	-17.12	0.75	0.51	24.58	12.48	1.0	0.	-30.3	12.1
0.3207	-16.75	1.01	0.	22.86	...	0.7	...	-65.1	11.6	...	1.
0.3209	-18.11	0.76	0.	19.74	...	0.3	...	-20.3	3.6
0.3217	-19.84	1.21	0.27	20.17	12.44	0.7	0.3	-6.3	4.3
0.3221	-18.15	1.73	0.	20.18	...	0.4	...	-2.6	0.9
0.3351	-19.60	1.40	1.	...	10.44	...	0.4	0.0	1.5	...	1.
0.3396	-19.29	1.66	1.	...	12.97	...	0.8	-5.9	-5.7	...	3.
0.3399	-18.61	1.35	1.	...	12.14	...	0.4	-6.4	5.4	...	0.
0.3471	-17.69	1.26	0.	19.01	...	0.1	...	-22.	0.
0.3474	-18.14	1.38	0.14	25.23	12.26	1.7	0.1	6.6
0.3474	-19.57	1.67	0.62	23.21	13.27	1.1	0.6	-1.4
0.3475	-18.65	0.82	0.	20.69	...	0.6	...	2.8
0.3476	-17.71	0.89	1.	...	11.76	...	0.2	-35.8
0.3477	-19.44	1.62	0.25	23.08	12.63	1.4	0.4	10.1
0.3479	-18.67	1.73	0.	16.63	...	0.6	...	5.5
0.3484	-18.42	1.33	0.	20.37	...	0.5	...	-13.4
0.3484	-19.18	1.37	0.48	20.75	15.77	0.6	1.	-3.6
0.3486	-17.49	0.59	0.	20.99	...	0.4	...	-40.9
0.3486	-19.25	1.09	1.	...	14.12	...	0.9	-17.0
0.3488	-20.22	1.73	0.51	21.28	12.18	0.9	0.4	-1.1
0.3546	-18.53	1.31	0.	21.09	...	0.7	...	-9.4
0.3697	-18.17	0.87	0.	21.52	...	0.7	...	-37.2
0.3829	-18.30	1.01	0.	19.65	...	0.4	...	-25.8
0.3830	-17.88	1.34	0.	20.08	...	0.3	...	-24.7	0.
0.3834	-18.24	0.90	0.35	26.48	11.96	1.8	0.2	-30.4	0.
0.3885	-19.99	0.20	0.	21.46	...	1.1	...	-16.1
0.3896	-19.99	0.35	0.18	19.71	13.88	0.7	0.6	-12.2	0.
0.3978	-18.38	1.10	0.	20.05	...	0.4	...	-17.4
0.3981	-18.45	1.41	1.	...	12.56	...	0.5	-16.4
0.3984	-17.95	0.81	0.	20.43	...	0.4	...	-28.3	1.
0.4032	-17.89	0.04	1.	...	12.17	...	0.5	9.8	1.
0.4091	-17.84	1.08	0.	21.47	...	0.6	...	-51.5	1.
0.4115	-19.45	1.22	0.	18.88	...	0.4	...	-17.0
0.4115	-18.68	1.01	0.	19.83	...	0.5	...	-12.5	0.
0.4274	-17.05	0.32	0.01	25.92	9.06	2.3	-0.7	6.5

Table 3—Continued

z	M_B	$(U-V)_0$	B/T	μ_{disk}	μ_{bulge}	Scl.ht log(kpc)	1/2lt rad log(kpc)	$[OII]$ (\AA)	H_δ (\AA)	D4000	Int level
0.4349	-18.09	1.39	1.	...	15.16	...	1.3	-14.7
0.4359	-19.88	1.38	0.22	18.29	7.49	0.4	-0.7	-2.9	0.
0.4548	-18.73	1.11	0.	19.57	...	0.4	...	-23.5	3.
0.2099	-17.52	0.83	0.	21.08	...	0.1	1.5	...	1.
0.2067	-17.08	0.91	0.	22.56	...	0.5	4.3	...	1.
0.2061	-17.55	0.78	0.	21.87	...	0.5	2.2	...	2.
0.2113	-17.50	0.88	0.	20.3	...	0.2	8.8	...	0.
0.2462	-17.42	0.97	0.	22.03	...	0.5	...	-47.9	-2.9	1.37	1.
0.2656	-17.43	1.91	0.	21.68	...	0.5	2.6	2.02	1.
0.2064	-17.57	0.95	0.	20.91	...	0.3	8.9	...	2.
0.2516	-17.74	0.82	0.	20.8	...	0.3	8.2	1.68	1.
0.2210	-17.66	2.05	0.02	21.13	13.95	0.4	-0.5	...	-0.2	...	0.
0.2065	-17.67	0.71	0.	21.43	...	0.4	1.1	...	0.
0.2428	-17.60	0.53	0.	21.96	...	0.6	4.2	1.09	0.
0.2221	-18.12	1.92	0.79	22.25	9.95	0.3	-0.5	...	7.0	...	0.
0.2583	-17.78	1.97	0.	20.28	...	0.2	2.1	1.93	0.
0.2076	-17.77	1.26	0.06	20.	12.43	0.2	-0.6	-37.5	10.6	1.14	0.
0.2090	-17.86	1.48	0.	20.65	...	0.3	...	-60.9	1.7	1.61	0.
0.2079	-17.30	1.63	0.47	21.64	19.59	0.4	1.3	-111.4	1.2	1.22	0.
0.2561	-17.76	1.65	0.	21.84	...	0.6	1.9	1.32	3.
0.2673	-17.93	0.45	0.	21.15	...	0.4	1.3	1.02	0.
0.2315	-17.85	1.47	0.	19.38	...	0.1	...	-26.4	-0.7	1.75	...
0.2646	-17.45	0.73	0.	20.01	...	0.2	...	-46.2	5.1	1.43	0.
0.1948	-17.88	1.14	0.	19.23	...	0.1	5.4	...	1.
0.2103	-18.10	1.01	0.62	22.36	9.66	0.5	-0.6	...	2.1	...	0.
0.2045	-18.31	1.07	0.	20.01	...	0.2	6.4	...	2.
0.2669	-17.81	1.37	0.	21.43	...	0.5	7.7	1.52	0.
0.2674	-18.09	1.07	0.	20.21	...	0.3	3.5	1.43	0.
0.2435	-18.02	1.35	0.	20.26	...	0.3	...	-43.9	8.9	1.67	0.
0.2028	-18.18	1.56	0.	19.93	...	0.2	...	-22.5	4.5	1.83	0.
0.2380	-18.10	1.93	1.	...	12.22	...	0.3	...	11.8	...	0.
0.2655	-17.85	1.71	1.	...	14.33	...	0.5	...	1.3	1.84	1.
0.2064	-18.34	1.31	0.	21.24	...	0.5	4.2	...	3.
0.2579	-17.95	0.71	0.	21.3	...	0.5	...	-51.3	4.0	1.48	1.
0.2210	-18.42	1.98	1.	...	11.09	...	0.1	...	2.2	...	1.
0.2032	-18.12	1.26	1.	...	12.65	...	0.3	-13.6	5.5	1.88	1.
0.2442	-17.89	0.48	0.	20.23	...	0.3	...	-76.2	15.4	1.43	2.
0.2656	-18.42	1.90	0.	21.5	...	0.6	5.4	1.62	2.
0.2301	-18.45	0.88	0.	21.04	...	0.5	7.9	...	1.
0.2237	-18.66	1.87	0.43	21.34	9.77	0.5	-0.5	...	7.8	...	3.
0.2390	-18.43	0.58	0.	21.49	...	0.6	1.8	...	1.
0.2260	-18.57	1.04	0.22	21.16	15.88	0.5	0.5	...	5.9	...	0.
0.2250	-18.74	2.15	0.41	22.33	9.78	0.7	-0.5	...	3.1	...	2.
0.2109	-18.56	1.32	0.	19.35	...	0.2	6.3	...	0.
0.2206	-18.60	1.92	1.	...	12.59	...	0.6	-14.4	2.2	1.82	3.
0.2255	-18.51	1.62	0.42	20.47	9.71	0.3	-0.5	...	3.3	...	0.
0.2509	-18.54	1.44	0.21	19.68	10.58	0.2	-0.5	...	1.3	1.73	0.

Table 3—Continued

z	M_B	$(U-V)_0$	B/T	μ_{disk}	μ_{bulge}	Scl.ht log(kpc)	1/2lt rad log(kpc)	$[OII]$ (\AA)	H_δ (\AA)	D4000	Int level
0.2545	-18.54	1.71	0.	20.85	...	0.5	2.2	1.39	0.
0.2083	-18.71	1.69	0.29	21.96	14.01	0.7	0.3	0.9	3.5	1.44	1.
0.2654	-18.28	0.97	0.	21.24	...	0.6	...	-14.1	1.9	1.91	1.
0.2096	-18.76	1.77	1.	...	12.35	...	0.3	...	7.4	...	1.
0.2304	-18.64	1.25	0.	20.14	...	0.4	6.2	...	0.
0.2685	-18.51	0.81	0.	19.46	...	0.2	3.6	1.61	0.
0.1928	-18.75	0.89	0.	21.18	...	0.6	8.2	...	1.
0.2068	-18.68	1.03	0.	22.52	...	0.9	6.5	...	1.
0.2244	-18.62	1.50	0.53	21.16	12.67	0.4	0.1	...	2.3	...	0.
0.2495	-18.80	1.70	1.	...	11.7	...	0.3	1.
0.2000	-18.67	0.64	0.	20.79	...	0.5	11.5	...	4.
0.2250	-18.71	1.45	0.33	19.82	10.49	0.2	-0.4	...	7.2	...	0.
0.2461	-18.84	0.82	0.	20.4	...	0.4	6.3	1.82	0.
0.2544	-18.52	1.61	1.	...	11.68	...	0.2	3.3	0.5	2.30	0.
0.2213	-18.82	1.74	0.18	20.42	11.64	0.4	-0.3	...	4.9	...	0.
0.2597	-18.64	1.53	1.	...	12.33	...	0.4	...	2.3	2.62	0.
0.1912	-18.98	2.00	0.66	22.69	14.63	0.7	0.6	...	-0.6	...	0.
0.2069	-19.02	2.06	1.	...	11.75	...	0.4	8.5	3.6	2.97	0.
0.2126	-18.71	1.64	0.27	20.32	19.44	0.4	1.4	-0.5	9.4	1.81	1.
0.2469	-18.78	0.98	0.	20.95	...	0.6	...	-16.6	8.4	1.65	0.
0.2446	-18.71	1.25	0.13	21.25	15.69	0.6	0.5	...	3.9	1.43	4.
0.2235	-18.97	1.01	0.	21.21	...	0.7	4.3	...	1.
0.2247	-19.09	2.06	0.38	21.63	10.3	0.6	-0.4	...	-0.4	...	1.
0.2059	-19.06	1.72	0.58	19.83	13.2	0.2	0.3	...	0.2	...	0.
0.2114	-19.05	1.85	0.37	21.03	9.3	0.5	-0.6	...	0.4	...	1.
0.2599	-18.54	0.69	0.	20.54	...	0.5	...	-7.5	5.9	1.66	0.
0.2485	-18.91	1.60	0.29	20.56	9.76	0.5	-0.5	...	2.	2.41	0.
0.2163	-18.57	0.87	0.05	21.35	10.04	0.7	-0.9	-15.8	2.7	1.48	1.
0.2060	-18.81	1.52	0.03	21.75	10.27	0.8	-0.9	-24.5	6.5	1.97	0.
0.2656	-19.21	1.91	0.55	21.37	12.11	0.5	0.1	-15.6	3.8	2.00	0.
0.2215	-19.49	2.09	0.	19.77	...	0.4	3.8	...	0.
0.2442	-19.01	1.40	0.	21.89	...	0.8	5.1	1.72	2.
0.2347	-19.06	1.47	0.	20.26	...	0.5	4.1	...	3.
0.2199	-19.20	1.03	0.	21.12	...	0.7	3.7	...	1.
0.2134	-19.15	1.50	0.	21.26	...	0.7	...	-5.2	4.7	1.53	2.
0.2099	-19.26	1.79	0.28	20.43	17.77	0.5	1.1	-2.4	2.7	1.72	0.
0.2068	-19.32	1.50	0.07	21.2	10.77	0.7	-0.6	...	4.4	...	1.
0.2393	-19.14	1.23	1.	...	14.1	...	0.8	...	6.5	...	0.
0.2658	-19.15	2.09	1.	...	13.76	...	0.7	...	0.8	2.02	0.
0.2210	-19.46	2.04	0.21	21.55	11.4	0.7	-0.2	...	3.6	...	1.
0.2508	-19.29	1.21	0.	21.05	...	0.7	3.0	2.07	0.
0.2279	-19.33	1.91	1.	...	13.45	...	0.7	9.4	4.7	2.12	2.
0.2478	-19.28	1.62	0.45	22.46	13.93	0.9	0.5	...	3.	2.33	0.
0.2166	-19.04	1.20	0.23	21.9	15.99	0.8	0.8	-2.4	8.3	1.57	3.
0.2117	-19.25	1.98	1.	...	13.31	...	0.7	-2.6	2.4	2.39	2.
0.2427	-19.07	1.22	0.	19.81	...	0.5	...	-20.	4.9	1.67	2.
0.2224	-19.63	2.06	0.35	21.48	8.95	0.7	-0.5	...	0.7	...	0.

Table 3—Continued

z	M_B	$(U-V)_0$	B/T	μ_{disk}	μ_{bulge}	Scl.ht log(kpc)	1/2lt rad log(kpc)	[OII] (Å)	H_δ (Å)	D4000	Int level
0.2223	-19.46	1.93	1.	...	13.85	...	0.7	-8.0	5.7	2.61	2.
0.1920	-19.60	1.23	0.15	21.69	14.08	0.8	0.3	...	3.0	...	3.
0.2374	-19.48	1.75	1.	...	11.78	...	0.3	-2.9	2.8	1.89	2.
0.2078	-19.69	1.55	1.	...	12.12	...	0.4	...	2.0	...	4.
0.2659	-19.64	2.01	0.35	20.71	13.3	0.6	0.4	...	-1.0	2.08	0.
0.2202	-19.64	1.46	0.11	20.41	9.97	0.6	-0.5	...	3.7	...	0.
0.2593	-19.55	1.40	0.1	19.76	10.26	0.5	-0.5	...	1.6	2.19	1.
0.2550	-19.76	0.95	0.06	21.45	10.87	0.8	-0.5	...	-0.6	1.17	3.
0.1901	-19.35	1.47	0.	20.99	...	0.8	8.3	1.48	4.
0.2047	-19.50	1.12	0.	20.04	...	0.6	...	-9.3	12.6	1.9	0.
0.2670	-19.73	1.29	0.	20.78	...	0.8	3.4	1.51	0.
0.2461	-19.94	1.61	0.27	20.95	13.72	0.8	0.5	-56.	-1.3	2.02	2.
0.2185	-20.11	1.81	0.	21.29	...	0.9	...	-5.0	4.7	1.61	1.
0.2481	-19.91	1.77	1.	...	15.72	...	1.5	...	2.7	3.17	3.
0.2676	-20.26	2.11	0.44	22.51	13.18	1.1	0.5	...	-0.4	2.26	2.
0.2178	-20.12	1.56	0.16	20.53	13.61	0.8	0.4	0.9	3.5	2.03	1.
0.2271	-20.51	2.11	1.	...	13.62	...	0.9	...	0.9	...	1.
0.2551	-20.30	1.55	0.76	19.84	14.77	0.4	1.	-3.7	6.9	2.01	3.
0.2243	-20.42	1.87	0.38	21.99	15.04	1.0	0.9	...	1.2	...	1.
0.2658	-20.42	1.63	0.11	21.29	9.49	1.0	-0.4	-12.9	5.3	1.96	0.

References

Abraham R.G. et al, 1996, ApJ, 462, 96

Carlberg R.G. et al, 1996, ApJ, 462, 32

Hutchings J.B., and Neff S.G., 1991, AJ, 101, 434

Morris S.L. et al, 1998 ApJ, 507, 84

Saintonge A., Schade D., Yee H.K.C., Carlberg R., Ellingson E., 2001 (in preparation)

Schade D., Lilly S.J., LeFevre O., Hammer F., Crampton D., 1996, ApJ, 464, 79

Captions to Figures

1. Spatial distribution of A2390 cluster galaxies in this paper. The Declination scale is exaggerated for clarity. Upper panel shows the MOS sample, which was used in all other diagrams, separated into the 3 principal morphology groups. The lower panel shows the other imaging samples. These are less extensive but were used for independent checks on the morphology results.

2. Bulge to disk ratios for cluster and field galaxies for A2390. Model errors in B/T are typically ± 0.08 or less.

3. Disk surface brightness and intrinsic-colour distributions for A2390 cluster and field galaxies. The dotted lines are the mean values for the field sample. Note the comparative lack of low surface brightness disks in the blue cluster galaxies. Model error bars typically 0.2 magnitudes, or about twice the size of the dots.

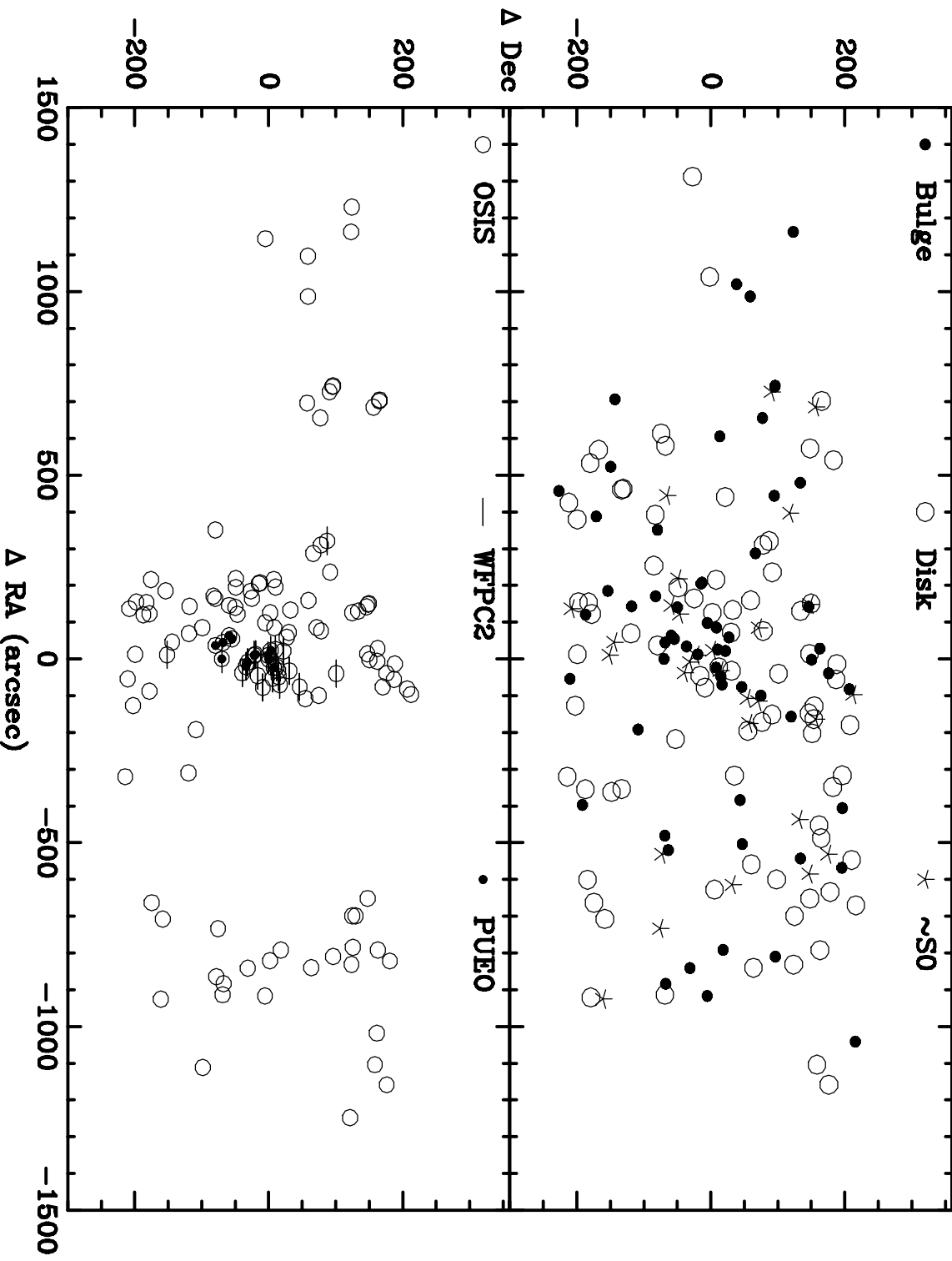
4. Disk scale-length changes with galaxy luminosity for A2390 and field galaxies. The dotted line is the linear fit to the field distribution, and the dashed line is the parabola fit to the cluster sample. Scale length error bars are typically 15%, about 0.1 in the log scale plotted.

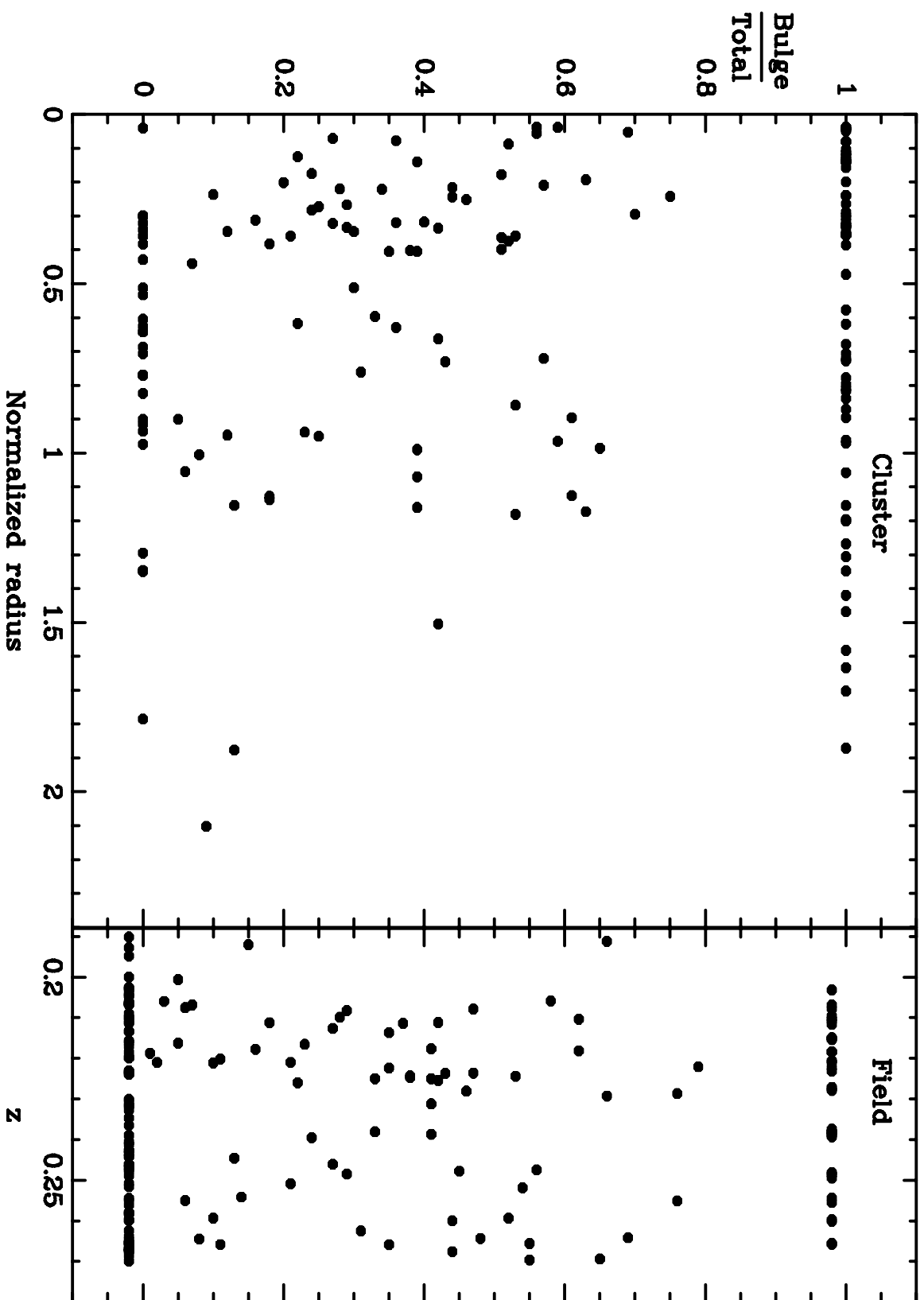
5. The fraction of cluster galaxies by morphology type for 4 bins of local galaxy density. The galaxy density is strongly correlated with radius within the cluster, as indicated by the R_{norm} values. The middle two bins are where there is significant degeneracy between radius and local density, as result of galaxy substructure, and have equal numbers of galaxies.

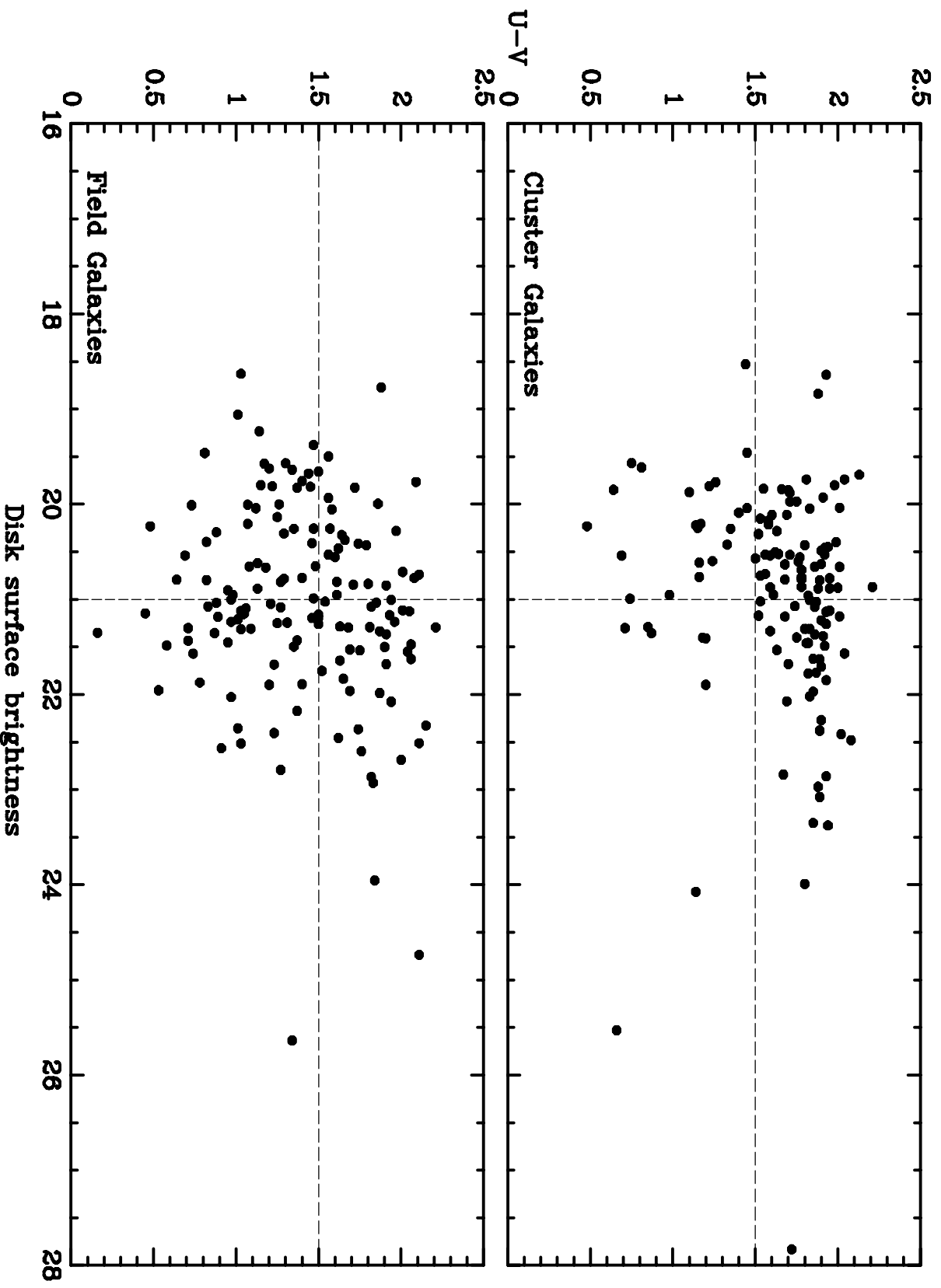
6. Spectroscopic quantities (from Abraham et al 1996) as a function of bulge to disk ratio for A2390 cluster and field galaxies.

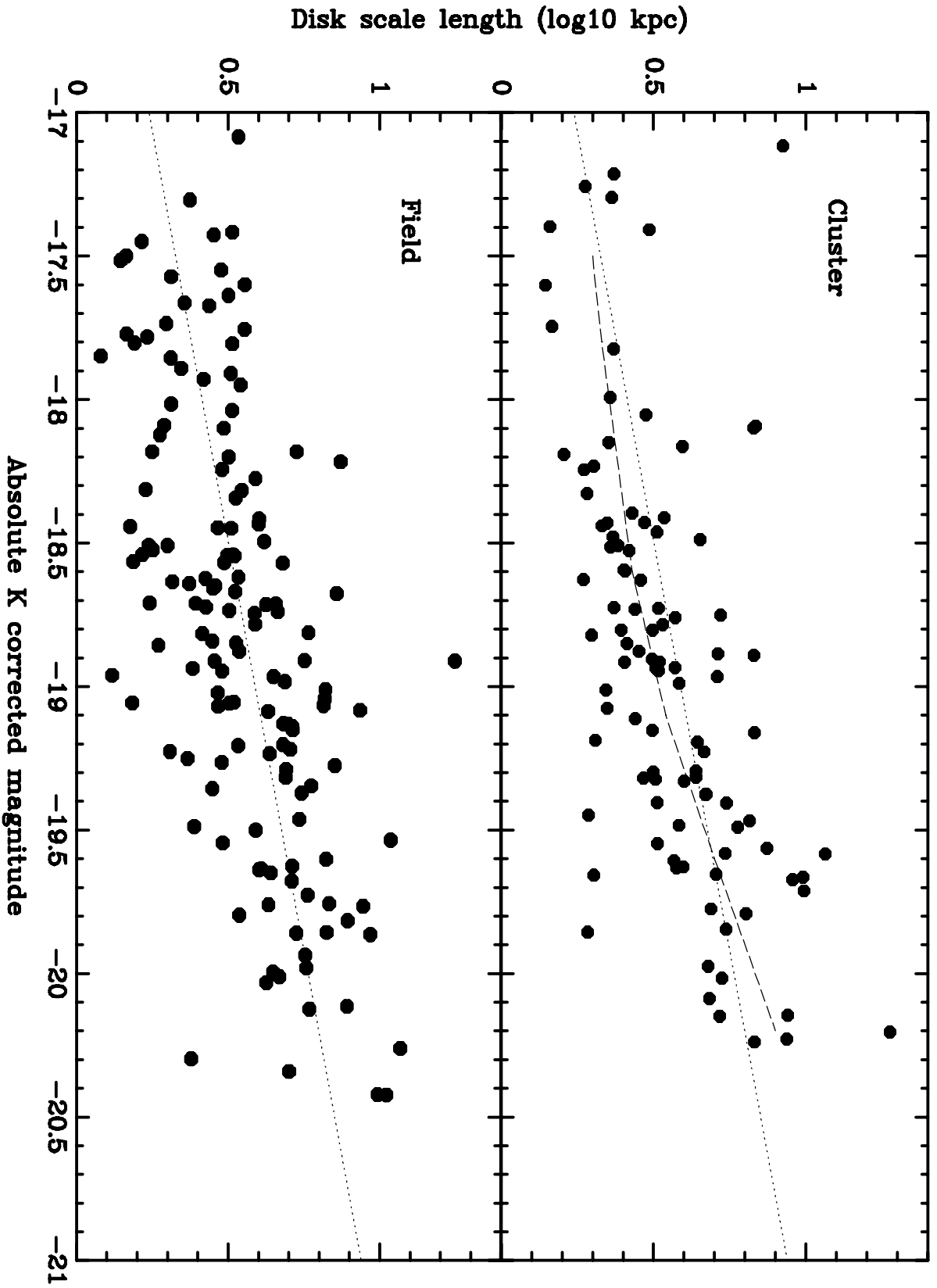
7. Spectroscopic quantities for A2390 cluster and field galaxies as function of 5-point interaction scale. The circles show the mean values for each group, and the percentages in the right panel refer to the full numbers of the cluster and field samples.

A2390 morphology









A2390 morphology

